Preprints of the 10th IFAC International Symposium on Dynamics and Control of Process Systems
The International Federation of Automatic Control
December 18-20, 2013. Mumbai, India

Sensor Fault Accommodation Strategies in Multi-rate Sampled-Data Control of Particulate Processes

Trina G. Napasindayao, Nael H. El-Farra*

* *Department of Chemical Engineering & Materials Science, University of California, Davis, CA 95616 USA (e-mail: nhelfarra@ucdavis.edu)*

Abstract: This paper focuses on the problem of handling sensor faults in controlled particulate processes with multi-rate sampled-data measurements. The problem is addressed on the basis of an approximate finite-dimensional system that captures the dominant dynamics of the infinite-dimensional particulate process system. An observer-based output feedback controller with an inter-sample model predictor is initially designed. The inter-sample model predictor provides the observer with estimates of the unavailable outputs, and its predictions are corrected each time that a measurement becomes available. Owing to the different sampling rates of the measurement sensors, the model update is performed using different outputs, or combinations of outputs, at each update time. The combined discrete-continuous closed-loop system is analyzed, and an explicit characterization of the feasible combinations of output sampling rates, model uncertainty, as well as controller and observer design parameters is obtained. This characterization is used as the basis for the development of both passive and active fault-tolerant control strategies that preserve closed-loop stability in the presence of sensor faults. The results are illustrated using a simulated model of a non-isothermal continuous crystallizer.

Keywords: Sampled-data control, sensor faults, passive fault-tolerance, sensor reconfiguration, particulate processes

1. INTRODUCTION

Fault-tolerant control of particulate processes is a fundamental problem in agricultural, chemical, food, mineral, and pharmaceutical industries. This problem is significant since malfunctions in the control system components or process equipment can negatively impact the particle size distribution and thus harm the end product quality. This problem has received limited attention compared to the significant body of research work on the synthesis and implementation of feedback control systems on particulate processes (e.g., see Semino and Ray (1995); Hu et al. (2005); Christofides (2002); Doyle et al. (2003); Larsen et al. (2006); Du and Ydstie (2012) for some results and references in this area).

Major bottlenecks in the design of model-based fault-tolerant control systems for particulate processes include the infinite-dimensional nature of the process model as well as the complex and uncertain dynamics of particulate processes. An effort to address these problems was initiated in El-Farra and Giridhar (2008) where a methodology for the detection and handling of control actuator faults was developed based on low-order models that capture the dominant process dynamics. The results were generalized in Giridhar and El-Farra (2009) to address the problems of fault isolation and robustness to model uncertainty.

Various implementation issues arise in the design of any fault-tolerant control system. These include discrete and multi-rate sampling of the output measurements, as well as the possibility of sensor faults. Measurement availability is constrained by inherent limitations on data collection, processing and transmission capabilities of the measurement sensors. In particulate processes, sensor measurements of the dispersed and the continuous phase variables are typically available at discrete times. The control system may also make use of multiple outputs subject to different sampling rates. For instance, the dispersed phase properties may be collected using light scattering techniques whereas properties of the solute concentration in the continuous phase may be obtained from a refractometer. Ignoring these factors in process monitoring and controller design may erode the performance of the fault-tolerant control system. Hence, it is crucial that these be explicitly accounted for in designing the monitoring and control systems.

Furthermore, fault-tolerant control systems need to consider the type of fault that occurs to ensure proper handling. Faults are classified as sensor, actuator, or component faults depending on where they appear in the system. While existing fault-tolerant control methods for distributed parameter systems have focused largely on actuator and component fault diagnosis and compensation (e.g., see El-Farra and Ghantasala (2007); Armaou and Demetriou (2008); Ghantasala and El-Farra (2009); Mahmood and Mhaskar (2010); Napasindayao and El-Farra (2012)), sensor faults are commonly encountered in practice and need to be accounted for. This can be achieved through either passive or active fault-tolerant control techniques, as opposed to component faults which are typically handled via fault accommodation (Napasindayao and El-Farra (2012)).

In this work, we develop a model-based framework for fault-tolerant control of multi-rate sampled-data particulate processes with sensor faults based on a finite-dimensional approximation of the infinite-dimensional system. The model is used in designing a stabilizing observer-based output feedback controller with an inter-sample model predictor that compensates for the discrete availability of multi-rate measurements. A closed-loop stability analysis is conducted leading to an explicit characterization of the interdependencies linking the stabilizing sensor sampling rates to the size of the model uncertainty, the controller and observer design parameters, and the choice of the control configuration. The stability conditions are used to obtain, for each control configuration, a region of stability in terms of the feasible sampling periods. This is then used to predict the behavior of the sampled-data closed-loop system under a certain set of operating conditions. A passive or active sensor fault compensation scheme is then selected and devised accordingly. The proposed fault-tolerant control framework is illustrated using a simulated model of a non-isothermal continuous crystallizer.

2. MOTIVATING EXAMPLE

As a representative example of particulate processes, we introduce in this section a well-mixed non-isothermal continuous crystallizer which will be used throughout the paper to illustrate the design and implementation of the model-based fault detection and accommodation schemes. Particulate processes are characterized by the co-presence of a continuous and dispersed phase. The dispersed phase is described by a particle size distribution whose shape influences the product properties and ease of product separation. Hence, a population balance on the dispersed phase coupled with mass and energy balances for the continuous phase are necessary to accurately describe, analyze and control particulate processes. Under the assumptions of spatial homogeneity, constant volume, mixed suspension, nucleation of crystals of infinitesimal size, mixed product removal, and a single internal particle coordinate–the particle size (r); a dynamic crystallizer model can be derived:

$$\begin{aligned}
\frac{\partial n}{\partial t} &= \bar{k}_1(c_s - c)\frac{\partial n}{\partial r} - \frac{n}{\tau_r} + \delta(r-0)\bar{\epsilon}\bar{k}_2 e^{\left(\frac{-\bar{k}_3}{(c/c_s-1)^2}\right)} \\
\frac{dc}{dt} &= \frac{(c_0-\rho)}{\bar{\epsilon}\tau_r} + \frac{(\rho - c)}{\tau_r} + \frac{(\rho - c)}{\bar{\epsilon}}\frac{d\bar{\epsilon}}{dt} \\
\frac{dT}{dt} &= \frac{\rho_c H_c}{\rho C_p}\frac{d\bar{\epsilon}}{dt} - \frac{UA_c}{\rho C_p V}(T - T_c) + \frac{(T_0 - T)}{\tau_r}
\end{aligned} \tag{1}$$

where $n(r,t)$ is the number of crystals of radius $r \in [0,\infty)$ at time t per unit volume of suspension; τ_r is the residence time; c is the solute concentration in the crystallizer; ρ is the particle density; $\bar{\epsilon} = 1 - \int_0^\infty n(r,t)\pi\frac{4}{3}r^3 dr$ is the volume of liquid per unit volume of suspension; $c_s = -3\bar{T}^2 + 38\bar{T} + 964.9$ is the concentration of the solute at saturation computed using $\bar{T} = \frac{T-273}{333-273}$; c_0 is the concentration of solute entering the crystallizer; $\bar{k}_1$, $\bar{k}_2$ and $\bar{k}_3$ are constants; and $\delta(r-0)$ is the standard Dirac function. The term containing the Dirac function accounts for the nucleation of crystals of infinitesimal size while the first term in the population balance represents the particle growth rate. For typical values of the process parameters, the crystallizer exhibits highly oscillatory behavior due to the relative nonlinearity of the nucleation rate compared to the growth rate. This results in process dynamics that are characterized by an unstable steady-state surrounded by a stable periodic orbit. Thus, the control objective is to suppress the oscillatory behavior of the crystallizer in the presence of sensor faults. This is carried out by stabilizing the system at the open-loop unstable steady-state that corresponds to a desired crystal size distribution by manipulating one of the three available manipulated inputs: the solute feed concentration (c_0), the residence time (τ_r), or the coolant temperature (T_c). Measurements of the solute concentration (c) and the temperature (T) in the continuous crystallizer are collected discretely at different sampling times and sent to the controller where the control action is calculated and then sent to the actuator to effect the desired change in the process state.

Through method of moments, a sixth-order ordinary differential equation system can be derived to describe the temporal evolution of the first four moments of the crystal size distribution, the solute concentration, and the temperature. The reduced-order model can be cast in the following form:

$$\begin{aligned}
\frac{d\mu_0}{dt} &= \frac{-\mu_0}{\tau_r} + \left(1 - \frac{4}{3}\pi\mu_3\right)k_2 e^{\frac{-k_3}{\left(\frac{c}{c_s}-1\right)^2}} e^{\frac{-E_b}{RT}} \\
\frac{d\mu_v}{dt} &= \frac{-\mu_v}{\tau_r} + v\mu_{v-1}k_1(c - c_s)e^{\frac{-E_g}{RT}}, v = 1,2,3 \\
\frac{dc}{dt} &= \frac{c_0 - c - 4\pi k_1 e^{\frac{-E_g}{RT}}\tau_r(c-c_s)\mu_2(\rho - c)}{\tau_r\left(1-\frac{4}{3}\pi\mu_3\right)} \\
\frac{dT}{dt} &= -\frac{4\pi}{3}\frac{\rho H_c}{\rho C_p}\frac{d\mu_3}{dt} - \frac{UA_c}{\rho C_p V}(T - T_c) + \frac{(T_0 - T)}{\tau_r}
\end{aligned} \tag{2}$$

The global phase portrait of the system of (2) has a unique unstable equilibrium point surrounded by a stable limit cycle at $x^s = [\mu_0^s \quad \mu_1^s \quad \mu_2^s \quad \mu_3^s \quad c^s \quad T^s]^T = [0.0047 \quad 0.0020 \quad 0.0017 \quad 0.0022 \quad 992.95 \quad 298.31]^T$. Multi-rate sampled measurements of the solute concentration (c) and temperature (T) are used to control the process. For simplicity, we consider the problem on the basis of the linearization of the process around the desired steady state. The linearized process model takes the form:

$$\dot{x}(t) = Ax(t) + B_l u_l(t), \;\; y(t) = Cx(t) \tag{3}$$

where $x(t) = [x_1(t) \quad x_2(t)]^T$ is the vector of state variables; $x_2(t) := y(t)$ is the measured output vector; u_l, $l \in \{1,2,3\}$, is the active control configuration (manipulated input). The state vector is in deviation variable form, $x(t) = \chi(t) - x^s$, where $\chi(t) = [\mu_0(t) \quad \mu_1(t) \quad \mu_2(t) \quad \mu_3(t) \quad c(t) \quad T(t)]^T$; and A, B_l, and C are constant matrices given by:

$$A = \left.\frac{\partial f}{\partial x}\right|_{(x^s,u^s)} = \begin{bmatrix} A_{11} & A_{12} \\ A_{21} & A_{22} \end{bmatrix}, \; B_l = \left.\frac{\partial f}{\partial u_l}\right|_{(x^s,u^s)} = [B_{l,1}^T \;\; B_{l,2}^T]^T,$$

and $C = \begin{bmatrix} 0 & 0 & 0 & 0 & 1 & 0 \\ 0 & 0 & 0 & 0 & 0 & 1 \end{bmatrix}$,

where u^s denotes the steady state values for the available manipulated inputs. Over the next two sections, we describe how the control strategy is tailored to explicitly account for the effects of multi-rate measurement sampling.

3. MULTI-RATE SAMPLING MECHANISM

Before designing and analyzing the control system with multiple measurement sampling rates, the time units (or intervals) in the multi-rate sampling mechanism are redefined to simplify the presentation and analysis of the results. We first define the sampling periods for the different sensors as $\Delta_1 = \delta_1\tau, \cdots; \Delta_m = \delta_m\tau$, where $\delta_1, \cdots, \delta_m$ are some positive integers. The following time units can then be obtained:

- Shortest time unit (STU): $\tau_s = \mathbf{gcd}(\delta_1, \delta_2, \cdots, \delta_m)\tau$, where $\mathbf{gcd}(\cdot)$ represents the greatest common divisor.
- Basic time unit (BTU): $\tau_B = \mathbf{lcm}(\delta_1, \delta_2, \cdots, \delta_m)\tau$, where $\mathbf{lcm}(\cdot)$ represents the least common multiple.

Using these two time units to analyze the multi-rate measurement sampling logic, output measurements may be collected and transmitted at a certain $\tau_j^k = (kM+j)\tau_s$, where τ_j is a possible sampling time (PST), $k \in \{0, 1, \cdots\}$, $j \in \{0, 1, \cdots, M-1\}$, and $M = \tau_B/\tau_s$. This order of sensor transmissions is repeated in a periodic fashion for each τ_B wherein all sensors are activated in the same patten in each $t \in [\tau_j^k, \tau_j^{k+1})$. Specifically, only at any τ_0^k, $k \in \{0, 1, 2, \cdots\}$, will all the sensors be activated concurrently. It should also be noted that the sensors can measure the outputs only at a PST; however, for some τ_j^k, not all the sensors are necessarily active. To indicate the sensor sampling status, we define a binary function $\varsigma(i, j)$ to show whether the i-th sensor is active or dormant at each PST τ_j^k:

$$\varsigma(i,j) = \begin{cases} 1, \text{ if } j \text{ is divisible by } \delta_i \\ 0, \text{ otherwise} \end{cases} \tag{4}$$

where $\varsigma(i, j) = 1$ if the i-th sensor transmits a measurement, while $\varsigma(i, j) = 0$ if the i-th sensor is dormant.

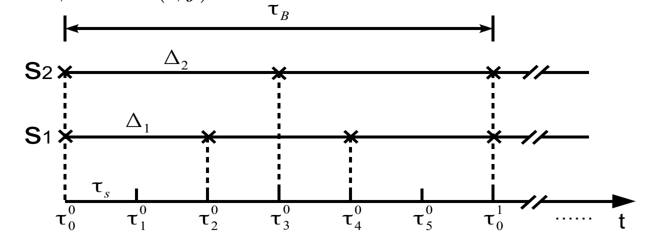

Fig. 1. Sampling schedule of two sensors with different sampling rates.

To illustrate the utility of this time unit system, consider a simple example involving two sensors with different sampling periods, $\Delta_1 = 0.2$ and $\Delta_2 = 0.3$. Based on the time unit notions introduced above, $\delta_1 = 2$, $\delta_2 = 3$, $\tau = 0.1$, and thus the STU is $\tau_s = 0.1$ while the BTU is $\tau_B = 0.6$. Based on this, the PSTs are $\tau_j^k = 0.1(6k + j) = 0.1\vartheta$, for $j \in \{0, 1, \cdots, 5\}$, $k \in \{0, 1, \cdots\}$, $\vartheta = 6k + j$. Comparing this result with the actual sampling times, it can be seen that the set of actual sampling times is a subset of the set of PSTs. This is concluded after investigating the sampling status at the first six PSTs in Fig.1. At $t = 0$, both sensors transmit their measurements to the controller; at $t = 0.1$ and $t = 0.5$, neither is active. Then at $t = 0.2$ and $t = 0.4$, only the first sensor is active; and at $t = 0.3$, sensor 2 is the only one that transmits the output measurement. This sampling pattern will be repeated over each $\tau_B = 0.6$ for all future times. This is only a specific example. Since the magnitude of the time units depends on the sampling periods of the sensors, each process will have a unique transmission schedule.

4. FINITE-DIMENSIONAL MULTI-RATE SAMPLED-DATA CONTROL SYSTEM DESIGN

4.1 Output feedback controller synthesis

The control system design involves first synthesizing an output feedback controller that stabilizes the finite-dimensional system when the sensors continuously transmit data to the controller. We consider an observer-based feedback controller of the form:

$$\begin{aligned} u_l(t) &= K\eta(t) \\ \dot{\eta}(t) &= \widehat{A}\eta(t) + \widehat{B}_l u_l(t) + L(y(t) - C\eta(t)) \end{aligned} \tag{5}$$

where η denotes the estimate of x, and $\widehat{A} = \begin{bmatrix} \widehat{A}_{11} & \widehat{A}_{12} \\ \widehat{A}_{21} & \widehat{A}_{22} \end{bmatrix}$ and $\widehat{B}_l = [\widehat{B}_{l,1}^T \quad \widehat{B}_{l,2}^T]^T$ are approximate models of A and B_l. Note that, in general, $\widehat{A} \neq A$ and $\widehat{B}_l \neq B_l$ to allow for possible model uncertainty. The controller (K) and observer gains (L) are chosen to ensure that the eigenvalues of $\widehat{A} + \widehat{B}_l K$ and $\widehat{A} - LC$ lie in the open left half of the complex plane.

4.2 Controller implementation under multi-rate sampling

The implementation of the controller of (5) requires continuous availability of all the measured outputs (y) from the sensors. The observer cannot be directly implemented since the output measurements are only partly available at discrete time instances due to multi-rate sampling. To compensate for the unavailability of continuous measurements, a low-order model of the system is included in the controller to provide the observer with estimates of the measured outputs when they are unavailable. In this case, however, not all the sensors send their measurements at a given time; instead, different sensors may transmit their data at different rates. When one or more sensors are active at a possible sampling time, the corresponding values of the measured outputs are assumed to be instantaneously transmitted to the controller and are used to update the corresponding model outputs and the model states. The model-based output feedback controller is then implemented as follows:

$$\begin{aligned} u_l(t) &= K\eta(t),\ t \in [\tau_j^k, \tau_{j+1}^k) \\ \dot{\omega}(t) &= \widehat{A}\omega(t) + \widehat{B}_l u_l(t),\ \widehat{y}(t) = C\omega(t) \\ \dot{\eta}(t) &= \widehat{A}\eta(t) + \widehat{B}_l u_l(t) + L(\widehat{y}(t) - C\eta(t)) \\ \widehat{y}^i(\tau_j^k) &= y^i(\tau_j^k),\ \forall\, \varsigma(i,j) = 1 \\ i &\in \{1, 2, \cdots, m\},\ j \in \{0, 1, \cdots, M-1\} \end{aligned} \tag{6}$$

where $\omega = [\omega_1(t) \quad \omega_2(t)]^T$ is the vector of model states which provides an estimate of x, $\omega_2(t) := \widehat{y}$ is the model output which provides an estimate of y, $\widehat{y}^i$ denotes the i-th element of $\widehat{y}$ and y^i represents the actual measured output of the i-th sensor.

4.3 Closed-loop stability analysis

To investigate the stability properties of the finite-dimensional sampled-data closed-loop system, we first define the model estimation error as $e^i(t) = \widehat{y}^i(t) - y^i(t)$, for $i \in \{1, 2, \cdots, m\}$, where e^i represents the difference between the i-th model output given in (6) and the actual measured i-th output. Then, introducing the error vector $e(t) = [e^1(t) \quad e^2(t) \quad \cdots \quad e^m(t)]^T$ and defining the augmented state vector $\xi(t) = [x(t) \quad \eta(t) \quad \omega_1(t) \quad e(t)]^T$, the finite-dimensional sampled-data closed-loop system can be formulated as a switched system and written in the form:

$$\begin{aligned} \dot{\xi}(t) &= F\xi(t),\ t \in [\tau_j^k, \tau_{j+1}^k) \\ e^i(\tau_j^k) &= 0,\ \forall\, \varsigma(i,j) = 1 \\ i &\in \{1, 2, \cdots, m\},\ j \in \{0, 1, \cdots, M-1\} \end{aligned} \tag{7}$$

where F is a matrix defined as

$$F = \begin{bmatrix} A & B_l K & O & O \\ LC & D & O & L \\ \widehat{A}_{12}C & \widehat{B}_{l,1}K & \widehat{A}_{11} & \widehat{A}_{12} \\ \widetilde{A}_{22}C - A_{21}\widehat{I} & O & \widehat{A}_{21} & \widehat{A}_{22} \end{bmatrix}, \tag{8}$$

$D = \widehat{A} + \widehat{B}K - LC$, $\widetilde{A}_{22} = \widehat{A}_{22} - A_{22}$, and $\widehat{I} = [I \ O]$ such that $x_1 = \widehat{I}x$ where I is the identity matrix. It can be shown that the augmented closed-loop system described by (7)-(8), subject to the initial condition $\xi(0) = [x(\tau_0^0) \ \ \eta(\tau_0^0) \ \ \omega_1(\tau_0^0) \ \ e(\tau_0^0)]^T := \xi_0$, has the following response:

$$\xi(t) = e^{F(t-\tau_j^k)} R^j N^k \xi_0 \tag{9}$$

for $t \in [\tau_j^k, \tau_{j+1}^k)$, $\forall\ j \in \{0, \cdots, M-1\}$, $k \in \{0, 1, \cdots\}$, where

$$\begin{aligned} R^j &= \Pi_{\mu=1}^{j} I_s^{j-\mu+1} e^{F\tau_s}, \ \text{ for } \ j \geq 1 \\ R^0 &= \text{diag}\{I,\ I,\ I\} \\ I_s^j &= \text{diag}\{I,\ I,\ I - S^j\} \\ S^j &= \text{diag}\{\varsigma(1,j),\ \varsigma(2,j),\ \cdots,\ \varsigma(m,j)\}, \end{aligned} \tag{10}$$

and N is given by:

$$N = I_s^0 e^{F\tau_s} R^{M-1} \tag{11}$$

The expressions in (9)-(11) characterize the multi-rate sampled-data closed-loop system behavior (in the absence of faults) in terms of the different sampling rates, the controller and observer design parameters, and the model uncertainty and the choice of control configuration. Based on (9)-(11), a necessary and sufficient condition for the stability of the sampled-data closed-loop system can be obtained. Specifically, by taking the norms of both sides of (9) and analyzing each term, it can be shown that the zero solution, $\xi = [x \ \eta \ e]^T = [0 \ 0 \ 0]^T$, is exponentially stable if and only if the spectral radius of the matrix N is strictly less than one, i.e., $r(N(\Delta_1, \cdots, \Delta_m)) < 1$. This requirement ensures stability by limiting the growth of the closed-loop state within each basic time unit of size τ_B as the sampling pattern is repeatedly executed over time.

An examination of the structure of N in (11) indicates that its spectral radius is dependent on the sampling periods, Δ_j, $j \in \{1, \ \cdots, \ m\}$, and F (which, in turn, depends on the choice of the model, the controller and observer gains, as well as the choice of manipulated input). All these factors are tied together through the stability condition which can, therefore, be used to examine and quantify the various interdependencies between them. For instance, if the sampling rate of a particular sensor is fixed by some performance requirement, one can determine the minimum allowable sampling rates of the other sensors. One can also use the result to characterize the robustness of a given sensor or actuator configuration to model uncertainty by identifying the range of model parameters that meet the stability criterion.

5. PASSIVE AND ACTIVE SENSOR FAULT-TOLERANT CONTROL STRATEGIES

In this section, we illustrate how the stability condition obtained in the previous section can be used to devise both passive and active sensor fault-tolerant control strategies. We focus on faults that degrade the sampling rate of the sensor and thus influence the rate at which the measurements are available to the controller. To this end, we revisit the non-isothermal continuous crystallizer example introduced in Section 2 where discrete measurements of the concentration (c) and temperature (T), which are available at different sampling rates, are used to control the system. The inter-sample model predictor is used to estimate values of the states as well as the outputs when the sensor measurements are unavailable. To account for plant-model mismatch, the model is designed with an uncertainty of $\delta_u = 0.2$ for the parameters k_w, $w = 1, 2, 3$ where $\widehat{k}_w = k_w(1 + \delta_u)$ is the approximate value used in the model.

The controller gain (K) is calculated by assigning the poles of $\widehat{A} + \widehat{B}_l K$ at $[-1 \ \ -2 \ \ -3 \ \ -4 \ \ -5 \ \ -6]$, while the observer gain (L) is chosen to place the poles of $\widehat{A} + LC$ at $[-10 \ -11 \ -12 \ -13 \ -14 \ -15]$. The system was controlled using one of three possible manipulated inputs: inlet solute concentration (c_0), coolant temperature (T_c), or residence time (τ_r). The stability regions were obtained for all possible manipulated variables using the stability condition $\lambda_{\max}(N) < 1$ (where $\lambda_{\max}(N)$ is the maximum eigenvalue magnitude of N), which was derived from the closed-loop stability analysis of the test matrix N in (11) (see Fig. 2). These regions, plotted as a function of the sampling periods for concentration (c) and temperature (T), differ significantly depending on the selected manipulated input. The green area enclosed by the unit contour line in each plot shows the region where the sampled-data closed-loop system is stable since $\lambda_{\max}(N) < 1$, while the yellow area depicts the region of instability. This characterization of the stability regions is useful in predicting the behavior of the process and in selecting an appropriate manipulated variable when the model uncertainty and sampling periods for the outputs are known (note that a plot of the stability region, while useful for visualization, is not necessary to make this determination since all that is needed to determine stability is to check the magnitude of the spectral radius of N for the given operating conditions).

Several conclusions can be drawn from a close inspection of the contour plots shown in Fig. 2. In this particular example, comparing the stability regions for the two cases when the inlet solute concentration (c_0) and the coolant temperature (T_c) is manipulated, it is evident that the stability region for the latter falls within that of the former (Figs. 2a,c). For this reason, the discussion on fault-tolerant control will focus on the use of the inlet solute concentration (c_0) and residence time (τ_r) as manipulated variables. In addition, it can be observed that the contour plots generated exhibit opposite trends when the inlet concentration (c_0) and when the residence time (τ_r) are being manipulated, wherein stability required small sampling periods for one configuration, and large sampling periods for the other. This pattern exhibited by the different stability regions can be utilized in devising actuator reconfiguration strategies wherein actuator switching is carried out to maintain stability when a back-up actuator is unavailable.

To illustrate the sensor fault-tolerance capabilities of the closed-loop system, we choose an initial operating point (OP) by setting a sampling period of $\Delta_1 = 0.002$h for the concentration sensor and $\Delta_2 = 0.008$h for the temperature sensor, which lies within the stability regions of both the c_0 and τ_r control configurations, and is therefore expected to be stabilizing. This is confirmed by the simulation results showing the evolution of the total particle size (Fig. 3a-b).

Although either control configuration may be used to control the crystallizer, robustness to faults in the measurement sensors is another criterion for selecting the best manipulated input. For instance, a close inspection of the two different regions of stability indicates that the process will be more robust to faults in the concentration sensor when the residence time (τ_r) is chosen as the manipulated variable (Fig. 2a-b). This is because this configuration has a wider range of possible sampling periods for the concentration sensor ($\Delta_2 < 1$h) that will lead to process stability at fast sampling rates for the temperature sensor ($\Delta_2 < 0.010$h) (Fig. 2b). Hence, if faults in the concentration sensor cause a deterioration in the sampling rate, closed-loop stability will not be lost. In contrast, manipulating the inlet solute concentration (c_0) results in greater tolerance for faults in the temperature sensor resulting in larger sampling periods (Fig. 2a).

Two scenarios will be used in the discussion below to show how fault-tolerance is achieved when the operating point lies within the region of stability which, in turn, is a function of the active manipulated variable, the initial operating conditions, and the magnitude and direction of the fault (i.e., a change in the sensor sampling period). In these examples, the faults are modeled by introducing a malfunction in one of the sensors resulting in a larger sampling period in either the concentration (c) or temperature (T) sensor. Different schemes are then proposed on how to best deal with each malfunction so as to maintain closed-loop stability.

In the first scenario, a malfunction occurs in the temperature sensor that shifts its sampling period from $\Delta_2 = 0.008$h to $\Delta_2 = 0.012$h (f_1). This pushes the operating point (OP:$\Delta_1 = 0.002$h,$\Delta_2 = 0.008$h) to a different location (f_1:$\Delta_1 = 0.002$h,$\Delta_2 = 0.012$h) in the stability regions (Fig. 2a-b). The new point is still within the region of stability when c_0 is manipulated (Fig. 2a). This, however, is not the case when τ_r is chosen as the manipulated variable (Fig. 2b). Closed-loop simulations of the dynamics of the system under the different manipulated inputs are in agreement with these predictions (Fig. 3c-d). When the process is initially operating using c_0 as the manipulated variable, the closed-loop system remains stable even after the fault takes place. The c_0 configuration is then passively fault-tolerant to the fault in the temperature sensor. In fact, a comparison of closed-loop state profiles shows that the system stabilizes much faster at the new operating point (Fig. 3a,c). This shows how carefully selecting the manipulated input results in passive fault-tolerance. Furthermore, the fault occurrence pushes the process into an operating point that now lies within the stability region when T_c is chosen as the manipulated input (Fig. 2c).

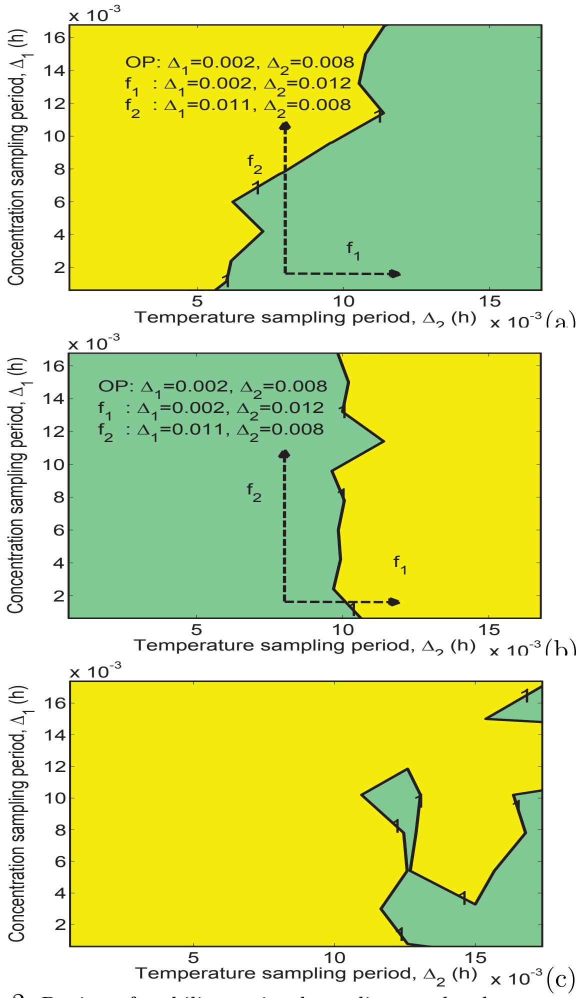

Fig. 2. Region of stability varies depending on the chosen manipulated input ($\delta_u = 0.2$). Plots (a)-(c): Contour plots of $\lambda_{\max}(N)$ when the manipulated variable is (a) inlet solute concentration, c_0; (b) residence time, τ_r; and (c) coolant temperature, T_c.

The coolant temperature (T_c) may then be used as a back-up actuator in case of an additional malfunction in the actuator manipulating c_0. However, to maintain stability after the sensor fault when the residence time (τ_r) is chosen as the manipulated input; the process has to either revert to a redundant temperature sensor with the original sampling period of $\Delta_2 = 0.008$h or switch to an actuator that manipulates either c_0 or T_c. Therefore, active reconfiguration of either the sensor or the actuator is necessary to maintain closed-loop stability for this control configuration.

The second scenario involves a malfunction in the concentration sensor that drives its sampling period from $\Delta_1 = 0.002$h to $\Delta_1 = 0.011$h (f_2). This moves the operating point (OP:$\Delta_1 = 0.002$h,$\Delta_2 = 0.008$h) to a different location (f_2:$\Delta_1 = 0.011$h,$\Delta_2 = 0.008$h) (Fig. 2a-b). This new point is still within the region of stability when the crystallizer is controlled using the residence time (τ_r) as the manipulated input, but outside the stability region of the two other control configurations (Fig. 3e-f). So, in this case, the τ_r control configuration is said to be passively fault-tolerant to the concentration sensor fault (notice that for sufficiently small fault size, the c_0 configuration may also be passively fault-tolerant, but the range of fault sizes it can tolerate is smaller than that for the τ_r configuration.) In the event of a malfunction in the mechanism used to manipulate the residence time (τ_r), there is no other option but active reconfiguration which may be carried out by either reverting to a back-up sensor to return to the initial operating point or switching to a different set of outputs that will move the operating point into a region of stability. Actuator reconfiguration may only be carried out by switching to a redundant actuator that manipulates the residence time (τ_r) since the new operating point is within the region of instability for both the c_0 and T_c configurations.

For the case where the process is initially controlled using c_0, the fault may be dealt with a number of ways: by switching to an actuator that manipulates the residence time (τ_r), returning to the original operating point using a redundant sensor, or using a different sensor with a different sampling period such that operating conditions are within a stable region. The last strategy is carried out by either selecting a temperature sensor with a larger sampling period or a concentration sensor with a faster sampling rate (Fig. 2b).

The contrast between the first and second scenarios indicates that a priori knowledge of the nature of future faults provides insight as to which manipulated input will be more robust to faults. An examination of the regions of stability indicate that the process is more robust to faults in the concentration sensor when the residence time (τ_r) is selected as the manipulated variable. If faults in the concentration sensor are projected to occur, then it would be wise to control the process by varying the residence time (τ_r) (Fig. 2b). If large faults in the temperature sensor are more likely to occur, then it is better to manipulate the inlet solute concentration (c_0) to make the process more robust to such faults (Fig. 2a). The same logic may be used with regards to knowledge of the sensors that are available for process monitoring. For instance, if temperature sensors with fast sampling rates are available, then it is better to manipulate the residence time (τ_r) while slow sampling rates for the temperature sensor work best when the inlet solute concentration (c_0) or coolant temperature (T_c) is manipulated.

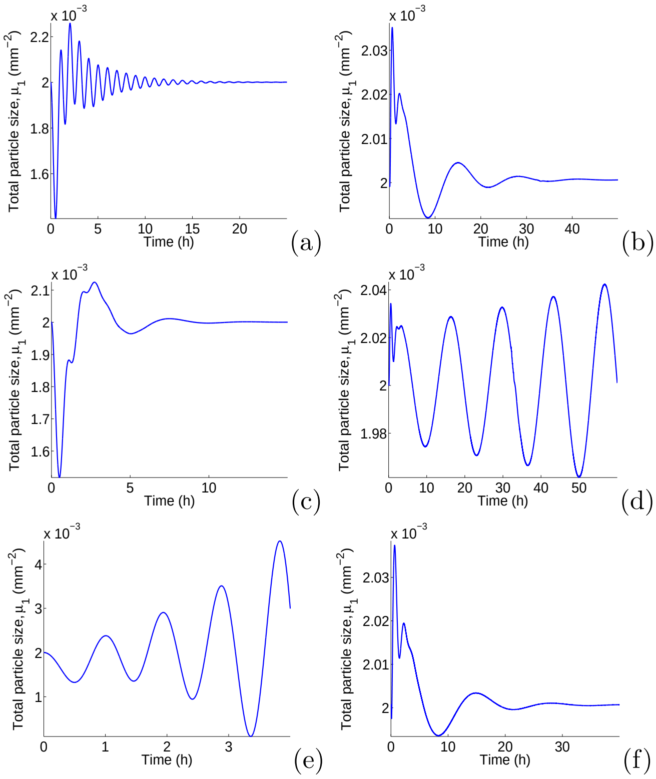

Fig. 3. Closed-loop state profiles depend on the selected manipulated variable ($\delta_u = 0.2$). Plots (a)-(b): Stability is reached when either (a) inlet concentration, c_0, or (b) residence time, τ_r, is manipulated (OP:$\Delta_1 = 0.002, \Delta_2 = 0.008$). Plots (c)-(d): System stabilizes when inlet concentration, c_0 (c), and not residence time, τ_r (d), is manipulated (f_1:$\Delta_1 = 0.002, \Delta_2 = 0.012$). Plots (e)-(f): System becomes unstable by manipulating either inlet concentration, c_0 (e), or residence time, τ_r (f) (f_2:$\Delta_1 = 0.011, \Delta_2 = 0.008$).

REFERENCES

Armaou, A. and Demetriou, M. (2008). Robust detection and accommodation of incipient component faults in nonlinear distributed processes. *AIChE J.*, 54, 2651–2662.

Christofides, P.D. (2002). *Model-Based Control of Particulate Processes*. Kluwer Academic Publishers, Netherlands.

Doyle, F.J., Harrison, C.A., and Crowley, T.J. (2003). Hybrid model-based approach to batch-to-batch control of particle size distribution in emulsion polymerization. *Comp. & Chem. Eng.*, 27(8-9), 1153–1163.

Du, J. and Ydstie, B. (2012). Modeling and control of particulate processes and application to poly-silicon production. *Chem. Eng. Sci.*, 67(1), 120– 130.

El-Farra, N.H. and Ghantasala, S. (2007). Actuator fault isolation and reconfiguration in transport-reaction processes. *AIChE J.*, 53, 1518–1537.

El-Farra, N.H. and Giridhar, A. (2008). Detection and management of actuator faults in controlled particulate processes using population balance models. *Chem. Eng. Sci.*, 63(5), 1185 – 1204.

Ghantasala, S. and El-Farra, N.H. (2009). Robust actuator fault isolation and management in constrained uncertain parabolic PDE systems. *Automatica*, 45, 2368–2373.

Giridhar, A. and El-Farra, N.H. (2009). A unified framework for detection, isolation and compensation of actuator faults in uncertain particulate processes. *Chem. Eng. Sci.*, 64(12), 2963 – 2977.

Hu, Q., Rohani, S., Wang, D., and Jutan, A. (2005). Optimal control of a batch cooling seeded crystallizer. *Powder Technology*, 156(2-3), 170–176.

Larsen, P., Patience, D., and Rawlings, J. (2006). Industrial crystallization process control. *Control Systems, IEEE*, 26(4), 70–80.

Mahmood, M. and Mhaskar, P. (2010). Safe-parking framework for fault-tolerant control of transport-reaction processes. *Ind. Eng. Chem. Res.*, 49(9), 4285–4296.

Napasindayao, T. and El-Farra, N.H. (2012). Fault detection and accommodation in particulate processes with delayed, sampled measurements. In *Proceedings of the 8th IFAC Symposium on Advanced Control of Chemical Processes*, 172–177. Singapore.

Semino, D. and Ray, W.H. (1995). Control of systems described by population balance equations-II. emulsion polymerization with constrained control action. *Chemical Engineering Science*, 50, 1825–1839.